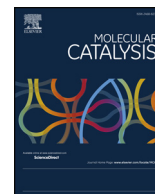




Contents lists available at ScienceDirect

## Molecular Catalysis

journal homepage: [www.elsevier.com/locate/mcat](http://www.elsevier.com/locate/mcat)

## Design of an optimized DRIFT cell/microreactor for spectrokinetic investigations of surface reaction mechanisms

Alejo Aguirre, Sebastián E. Collins\*

*Instituto de Desarrollo Tecnológico para la Industria Química (INTEC), Universidad Nacional del Litoral, CONICET, Güemes 3450, S3000GLN, Santa Fe, Argentina*

## ARTICLE INFO

## Keywords:

DRIFT microreactor  
Operando  
Surface reaction  
CO oxidation  
Gold catalyst

## ABSTRACT

A cell/microreactor is developed and fully characterized to perform diffuse reflectance infrared Fourier transform spectroscopy (DRIFTS) experiments to investigate heterogeneously catalyzed surface reactions. The experimental setup allows the simultaneous acquisition of time-resolved infrared spectra at high quality and the gas phase quantification by a mass spectrometer connected at the outlet of the cell. The cell behaves as a true plug-flow microreactor while allowing the infrared radiation to sense the lateral part of the catalyst bed. The selected geometry allows a better correlation between the evolution of infrared signals from surface species and the gas concentration at the exit of the cell, that is, for strict Operando experimentation. The mass and heat transport phenomena were characterized using well established criteria to determine the operative limitations under steady state and fast transient experiments, e.g. during concentration-modulation excitation spectroscopy (c-MES). The performance of the cell is validated by studying the CO oxidation on a Au/CeO<sub>2</sub> catalyst. Identification and quantification of active surface species under reaction conditions are obtained combining modulation approach with phase sensitive detection (PSD) analysis and step experiments.

### 1. Introduction

Understanding of reaction mechanisms and structure-activity relationships under working –Operando– conditions is of central importance to perform a rational design of new and optimized catalytic systems. Spectroscopic microreactors/cells to study reactions at the gas/solid interface have been developed and employed to a greater extent in the literature. For example, Raman cells [1], UV–vis [2], XAS [3–5] (X-ray absorption spectroscopy), XRD (X-ray diffraction) [3], UVvis / Raman [6,7], FTIR transmission [8–16] and DRIFT [17–22]. However, only few works have reported a systematic characterization of the system using the different criteria developed for reactor engineering [23].

For the identification and tracking of surface intermediates, infrared spectroscopy offers a wide range of advantages. Transmission IR techniques, using pressed catalyst wafers, are the traditional mode for catalysts characterization, particularly because it provides a high sensibility. However, mass transfer limitations on pressed wafers could hamper the catalyst observation under real “operando” conditions, that is, to observe the catalyst under real activity runs [15]. Diffuse Reflectance Infrared Fourier Transformed Spectroscopy (DRIFTS) offers the advantage that it allows collecting IR spectra from the powder catalyst while flowing gases through the catalyst bed. The high loss of the

radiation (95–98% of the incident beam), which reduces the S/N ratio, can be overcome by using high-sensitivity (and fast) MCT detectors. Moreover, DRIFT cells are easy to couple with analytical techniques such as gas chromatography or mass spectrometry.

In the last years, besides the operando (under steady state) requirements for reaction cells, new methodologies for transient (quantitative) investigations in heterogeneous catalysis impose more rigorous requirements for cells performance. For instance, periodic changes in feed composition (modulation excitation spectroscopy, MES) [24–30], rapid pulse reaction switching and pulse adsorption perturbations are also of particular interest for the determination of reaction mechanisms and to discriminate between active and spectator species [31]. In any case, very demanding instrumental design for the correct interpretation of collected spectral information is required. To this aim the correct design of cells/microreactors that allows the simultaneous acquisition of spectroscopic and kinetic data is of central importance. The design and testing of kinetically-appropriate operando spectroscopic cells for investigating heterogeneous catalytic reactions was reviewed by Meunier [23]. The effect of the probing radiations, temperature control and gradients in the cells, gas flow patterns and catalyst bed by-pass on wafers and powders was thoroughly analyzed. Later, the specific issue of temperature gradients in DRIFTS cells and catalyst bed was also addressed [32]. Thus, the major requirements needed to perform

\* Corresponding author at: INTEC-CONICET. Güemes 3450, Santa Fe, S3000GLN, Argentina.

E-mail address: [scollins@santafe-conicet.gov.ar](mailto:scollins@santafe-conicet.gov.ar) (S.E. Collins).

<https://doi.org/10.1016/j.mcat.2018.07.003>

Received 15 May 2018; Received in revised form 27 June 2018; Accepted 2 July 2018

2468-8231/ © 2018 Elsevier B.V. All rights reserved.

kinetic analysis in DRIFT can be summarized as follows: (i) small cell volume allowing rapid reactants exchange (ii) no dead volume (iii) minimal pressure drop, (iv) no temperature gradient in the catalyst bed, (v) optimized cell geometry to perform as a plug flow microreactor, and (vi) high surface of the sample exposed to the IR radiation to avoid excessive beam attenuation. Moreover, time and spatial resolution can also be convenient [20–22].

In this work, the design and rigorous characterization of a DRIFT cell that features a plug-flow microreactor, coupled with mass spectrometry to perform Operando and transient studies in a quantitative manner is described. As a proof of concept, the cell was used to study the oxidation of CO by DRIFT + MS on an Au/CeO<sub>2</sub> catalyst.

## 2. Experimental

### 2.1. Experimental setup

A stainless steel DRIFT cell/microreactor with small volume was design and constructed; and it is described in the following section. The cell was mounted into the Praying Mantis diffuse reflection accessory (Harrick) inside the sample compartment of the FTIR spectrometer (Thermo-Electron, Nicolet 8700 with a cryogenic MCT detector). The bench of the spectrometer was continuously purged with dried air (Parker Balston FTIR purge gas generator) to eliminate CO<sub>2</sub> and water vapor contributions to the spectra. Time-resolved DRIFT spectra were recorded at a resolution of 4 cm<sup>-1</sup> (up to 1 spectrum/0.39 s). The exit of the cell was connected to a mass spectrometer Prisma QMG220 (Pfeiffer) by a sampling capillary. The entrance of the gases was controlled by a flow-through 10-ways valve electronically actuated (Vici-Valco) synchronized with the FTIR. The flow rate was regulated by mean of mass flow meters (Cole-Parmer). Fig. 1 shows a simplified scheme of the experimental setup.

### 2.2. Catalyst and catalytic test

The CO oxidation reaction was studied over an Au(1.87wt%)/CeO<sub>2</sub> (57 m<sup>2</sup>/g) catalyst with an average gold particles of 1.4 nm (D<sub>Au</sub> = 65%) [33]. The cell was filled with 48 mg of the catalyst and 200 mg of milled quartz placed previous to the catalyst bed. Before the experiments, the catalyst was *in-situ* calcined by flowing O<sub>2</sub>(5%)/He at 423 K (5 K/min, 1 h, 50 mL/min), followed by purging with He (1 h, 50 mL/min) and cooling down in He up to 303 K. A light-off curve from 303 up to 423 K (5 K/min) was performed. The temperature was maintained at 423 K for 10 min and then cooled down to 303 K. The reaction mixture composition was CO(1%)+O<sub>2</sub>(0.6%) balanced with He (total flow rate = 50 mL/min). Subsequently, transient and modulated MES experiments were performed at 303 K. Details of the modulated MES experiments implementation and the data processing by phase sensitive detection (PSD) methodology can be found elsewhere [24] and in the Supplementary Information.

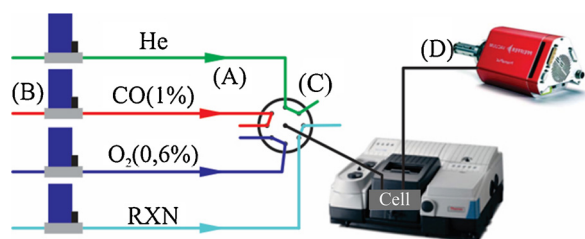


Fig. 1. Simplified scheme of the experimental setup: (A) low volume stainless steel connections; (B) mass flow meters; (C) through-flow 10-ways valve electronically actuated; (D) mass spectrometer.

## 3. Results

### 3.1. Design of the DRIFT microreactor

The most commonly used DRIFT cells features a heated cup where the catalyst powder is placed and the gas feed is, in the best situation, forced to flow through the catalyst bed (Figure S1). Commercial examples are Harrick®, Pike® and Spectra-Tech® DRIFT cells. These cells have some advantages in terms of temperature and pressure working ranges and also present high signal-to-noise ratio. It is important to highlight that in a spectroscopic cell design, it must be found a compromise between the performance as an ideal catalytic reactor and allowing the entrance of the radiation through a transparent window [23]. Several research groups have modified those designs to improve their performance, for example to avoid the bypass of the gases [17], to minimize dead-volume [18] and to improve the correct measurement of the catalyst temperature [19,32].

As pointed out in the introduction, the engineering aspects of the cell design must be considered with the aim of developing a spectroscopic cell that allows to perform operando studies under chemical control conditions, measuring simultaneously the concentration of the gas phase (products and reactants) and the concentration of superficial species [23]. One common problem is the large internal volume, limiting the implementation of transient experiments with fast reactant exchange or pulse experiments. For instance, the internal volume of the Harrick® cell, including the dome, is ca. 14 mL, which means that at a gas flow rate of 50 mL/min, the residence time ( $\tau$ ) is 16.8 s, *i.e.* the exchange of 99% of gas takes 77 s (see Supplementary Information Figure S2). Additionally, the presence of temperature gradients in the cell and in the catalyst bed has been thoroughly addressed by Meunier and co-workers [32]. Another critical aspect is where the IR beam is sensing the catalyst. In the commercial DRIFT cells, the IR beam is sensing the top part of the catalyst bed, penetrating around of 200  $\mu$ m [21]. However, during the reaction, the concentration of reactants varies along the catalyst bed and; therefore, the surface adsorbed species concentration varies too. Then, the infrared information could not be directly correlated with the products concentration measured at the exit of the cell- except at differential conversion-(see Supplementary Information Figure S1). Then, a solution to avoid this problem is that the IR beam sense longitudinally the catalyst bed, *i.e.* the IR beam hits the lateral side of the catalyst bed as was successfully implemented in Raman Operando Cell [1], and in two previously reported DRIFT/XAS [5], and DRIFT/Raman [21,22] cells.

Therefore, a DRIFT cell/microreactor in which kinetic analysis of heterogeneous catalyzed reactions under chemical control conditions and fast transient experiments can be performed, was designed. The following criteria were taken into account: (i) avoid temperature gradients in the catalytic bed, (ii) allow the measurement of the actual temperature in the catalyst bed, (iii) the volume of the cell should be small enough to allow rapid exchange of the reactants without dead volumes, (iv) allow to correlate the IR signals from surface species with the gas phase concentration at the cell exit, and (v) the area where the IR beam is focus must be representative of the adsorbed species concentration.

A scheme and picture of the designed DRIFT cell/microreactor are shown in Figs. 2 and 3 respectively. The cell body was made of stainless steel 316 L and in the top part was drilled a groove ( $2 \times 3 \times 15$  mm<sup>3</sup>), where the catalyst is deposited (A). A CaF<sub>2</sub> window (B) closes the upper part of the cell body adjusted to a Kalrez® seal (C). The seal is fixed in a seat (D) and can be heated up to 573 K. The inlet (E) and outlet (F) of the cell are made of 1/8" and 1/16" stainless steel tubes, respectively. The cell is heated by means of a 200 W heater cartridge placed in a hole drilled along cell body (G). The temperature control is made by means of two thermocouples: (i) one inserted in the catalyst body, directly below the catalyst bed (H) and (ii) another, with a diameter of 0.25 mm, inserted into the catalyst bed (J). With the aim to pre-heat the

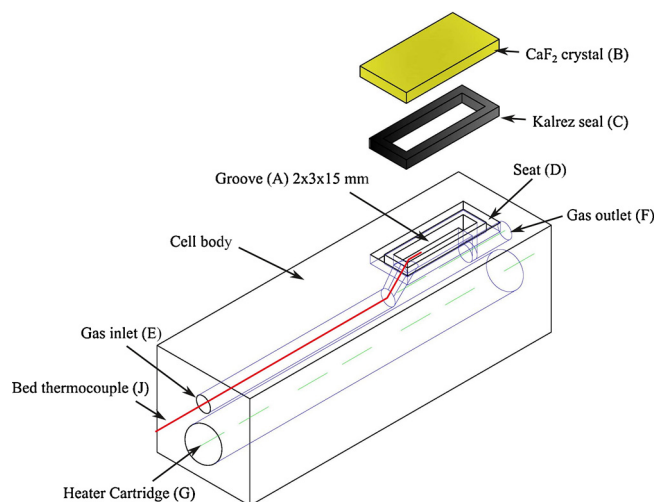


Fig. 2. Scheme of the DRIFT cell.

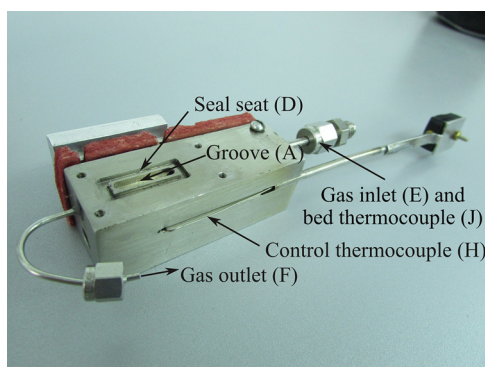


Fig. 3. Picture of the DRIFT cell.

fed gases, the inlet tube is filled with quartz (60 mesh). The problems of the dome high volume and dead volume zones in the Harrick cell, which produce a slow exchange of reactants, were previously described. In the new developed cell the dome was removed, placing the infrared window directly above the catalytic bed, which totally eliminates dead volumes.

### 3.2. Cell characterization

#### 3.2.1. Temperature measurement

As pointed out before, the correct measure of the actual catalyst temperature and avoiding temperature gradients are some of the most important issues to address for a proper behavior of the cell/microreactor. In the new cell, the temperature is measured directly in the catalyst bed using a 0.25 mm thermocouple. In order to verify experimentally the absent of temperature gradients in the catalyst bed a series of experiments were conducted changing the flow rate (100 and 20 mL/min), using gases with different conductivity (He and Ar) and varying the thermocouple position along the catalyst bed (front, middle and back). For this test, 60 mg of alumina (200 m<sup>2</sup>/g, 200–140 mesh) were placed into the cell. It is worth to note that before the catalyst bed, ca. 200 mg of milled quartz (60 mesh) is placed in order to pre-heat the inlet gases. Fig. 4 shows the comparison between the temperature measured in the catalyst bed and the set temperature. It is observed that there is no significant temperature change along the catalyst bed. The maximum temperature difference was  $\pm 2$  K at steady state and  $\pm 5$  K during the heating/cooling cycles (ramp of 5 K/min). Note that, with the aim of simplify the graphic visualization, only the results obtained with the thermocouple inserted at the beginning of the catalytic bed

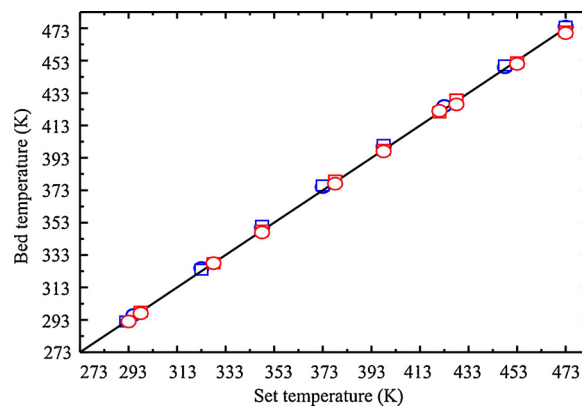


Fig. 4. Correlation between the temperature in the catalyst bed and the temperature measured by the control thermocouple (set temperature). The colors represent the gases: Ar (red) and He (blue); the symbols the flow rate: 100 mL/min (squares) y 20 mL/min (circles) (For interpretation of the references to colour in this figure legend, the reader is referred to the web version of this article.)

(worst condition) are shown. For the experiences with the thermocouple placed at the end of the bed the results were identical. These results show that the new design and the filling with milled quartz prior to the bed are effective for pre-heating the gases.

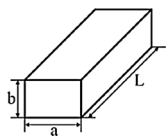

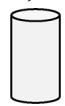
#### 3.2.2. Transport characterization

An analysis of the transport phenomena is presented by comparing the new optimized cell, a commercial cell (Harrick) and a 1/4" plug-flow glass reactor. Table 1 summarizes the geometry characteristics of each system. For the new DRIFT microreactor, the volume is 90  $\mu$ L with a flow section of 6 mm<sup>2</sup>. Note that the volume is calculated for the total length,  $L = 15$  mm, that is, for the groove completely filled with catalyst; however, it is possible to load less material by placing before and/or after the bed an inert filling material (e.g. milled quartz, quartz wool, etc.). Then, for a bed volume of 90  $\mu$ L, the commercial DRIFT cell has an aspect ratio ( $L/D_H$ ) of 0.55 and the tubular reactor of 1.8 (catalyst not diluted); while in the new cell the aspect ratio is 6.25.

The new cell has a smaller flow section than the tubular reactor, which produces a higher velocity of the gases. This higher flow velocity causes an increase in the mass and energy transfer coefficients (see next section) without changing the residence time of the reactor. For example, for a flow rate of 50 mL/min the average velocity in the cell is 13.9 cm/s while in the tubular reactor is 6.6 cm/s. Table 2 shows the

Table 1

Dimensions of the new cell, commercial cell and tubular reactor.

	New cell-microreactor	Commercial cell (Harrick™)	Tubular reactor (1/4")
			
V	90 $\mu$ L	14 mL (dome) ~ 90 $\mu$ L (cup)	90 $\mu$ L
$D_H$ (mm)	2.4	6	4
S (mm <sup>2</sup> )	6	28.27	12.56
Aspect relations	$L/b = 7.5$ $L/a = 5$ $L/D_H = 6.25$ $L/dp = 150$ $D_H/dp = 24$	$L/D_H = 0.55$ $L/dp = 30$ $D_H/dp = 60$	$L/D_H = 1.8$ $L/dp = 72$ $D_H/dp = 40$

V = volume, S = flow section,  $D_H$  = hydraulic diameter,  $D_H = 4x$ (Wet perimeter)/section.

**Table 2**

Characteristics and dimensionless numbers of the new and commercial cell and a tubular reactor.

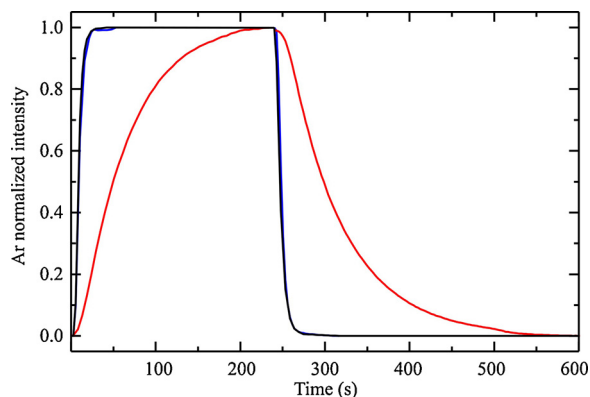
	New cell	Commercial cell	Tubular reactor (1/4")
$v_g$ (cm/s)	13.9	2.95	6.6
$\tau$ (s)	0.108	16.8 (dome) 0.108 (cup)	0.108
$Re_p = \frac{v_g \rho d_p}{\mu}$	0.8	0.2	0.4
$Pe_p = \frac{v_g d_p}{D_i}$	1.4	0.3	0.7
$Pe_L = \frac{v_g L}{D_i}$	209	10	48
$Pe_r = \frac{v_g D_H}{D_i}$	31.44	17.7	26.4

$v_g$  = gas velocity (free section),  $\tau$  = residence time,  $Re_p$  = particle Reynolds number,  $Pe_L$  axial Péclet number,  $Pe_r$  radial Péclet number y  $Pe_p$  particle Péclet number. Considering:  $Q_v = 50$  mL/min;  $d_p = 0,1$  mm;  $\rho = 1,1$  Kg/m<sup>3</sup>;  $\mu = 1,9 \times 10^{-5}$  Pa s;  $D_e = 0,1$  cm<sup>2</sup>/s.

average velocity for the cells and the reactor and the derived dimensionless numbers for a particle diameter,  $d_p = 0.1$  mm; a gas density,  $\rho = 1.1$  Kg/m<sup>3</sup>; a gas viscosity,  $\mu = 1.9 \times 10^{-5}$  Pa s; and an effective diffusion coefficient,  $De = 0.1$  cm<sup>2</sup>/s. The flow regime is laminar for the three cases due to the low Reynolds number ( $Re_p < 10$ ). Moreover, in the new DRIFT cell the axial Péclet ( $Pe_L$ ) and the radial Péclet ( $Pe_r$ ), which represent the relation of the transport by convection with the transport by diffusion, are larger than in the other cases indicating that the dispersion, both axial and radial, is minimized.

In order to study the fluid-dynamic behavior of the developed cell, a set of experiments were performed switching from Ar(2%)/He to He. Fig. 5 shows the gas concentration evolutions recorded by the mass spectrometer at the exit of the cell during the change from He to Ar (2%)/He and He again at a flow rate of 10 mL/min with the empty DRIFT cell (without catalyst), the commercial cell and the 1/4" tubular reactor as blank experiment. Fig. 5 shows that the response using the new cell is identical to the plug-flow reactor, reaching the maximum of the signal at 29 s. In contrast, the signal obtained in the commercial cell reaches the maximum only after ca. 240 s. Table 3 shows the times needed to reach the maximum of the signal for three different flow rates. Please, note that the exchange times measured experimentally with the MS include the volumes of the tubes before and after the cell. These volumes are greater than 90  $\mu$ L (new cell volume), so the exchanging time is greater than the residence time reported in Table 2.

The absence of dead volume in the optimized cell design allows a rapid change of reactants, which is essential to study rapid reactions



**Fig. 5.** Normalized signal evolution of Ar during a step experiment for a flow rate of 10 mL/min using the commercial cell (red) and the developed cell (blue). The black line is the blank experiment (For interpretation of the references to colour in this figure legend, the reader is referred to the web version of this article.).

**Table 3**

Exchange time of Ar(2%) for different flow rates.

Flow rate (mL/min)	Exchange time (s) <sup>a</sup>		
	New cell	Tubular reactor	Commercial DRIFT cell
10	29	28	240
20	11	10	150
50	8	8	85

<sup>a</sup> Time needed to reach the 99.5% of the signal maximum.

through transient experiments. In contrast, using the commercial cell it is impossible to generate stimulus at high frequency due to the large volume of the dome (ca. 14 mL). For instance, whether a MES experiment is carried out with a frequency of 16.67 mHz (valve change every 30 s) and with a flow rate of 50 mL/min, the Ar signal oscillates between 80 and 20% of its maximum value (Figure S3).

From another point of view, although the increase in the gas velocity improves the mass and heat external transfers (fluid-particle) and minimizes the effect of dispersion, a large increase in the gas velocity can cause a high pressure drop along the cell. The pressure drop in the DRIFT microreactor was measured for a series of He gas flow rates using a bed of 200 mg of ground quartz (60 mesh) and 60 mg of alumina ( $200 < dp < 140$  mesh). Figure S4 shows the measured pressure drop as a function of the flow rate for the empty cell (without catalyst) and for the cell with the catalytic bed. It is observed that the pressure changes linearly with the velocity, typical of the laminar regime (low Reynolds). The pressure drop is only 1 psi (7%) for a flow rate of 50 mL/min. This value is negligible in comparison with the intrinsic equipment errors (DRIFT + MS). The experiment shows that the pressure drop along the catalytic bed will not affect the quantitative measurements.

### 3.2.3. Operational limits

**3.2.3.1. Fluid-particle mass and heat transfer.** In order to evaluate the limitations of external mass and heat transfer, which could limit the correct determination of intrinsic kinetics of surface reaction intermediates, the transfer coefficients are calculated. The factors of Chilton-Colburn ( $j_D$  and  $j_H$ ) are used to calculate the fluid-particle transfer coefficients [34,35]

$$k_g = j_D \frac{G}{\rho} Sc^{-2/3} \quad (1)$$

$$h_f = j_H c_p G Pr^{-2/3} \quad (2)$$

where,  $G$  is the superficial gas velocity,  $Sc = \frac{\mu}{\rho D_i}$  is the Schmidt number,  $Pr = \frac{c_p \mu}{\lambda}$  is the Prandtl number,  $D_i$  is the solute diffusion coefficient,  $\mu$  is the fluid viscosity,  $\rho$  is the fluid density,  $c_p$  is the heat capacity, and  $\lambda$  is the thermal conductivity. As an example, considering He as dilution gas, cerium oxide (see next section) as the solid catalyst with a particle diameter of 0.1 mm and a flow rate of 50 mL/min, the fluid-particle transfer coefficients are: mass transfer coefficient,  $k_g = 14.8$  m/s and heat transfer coefficient,  $h_f = 1702$  W/(m<sup>2</sup> K). Then, the maximum measurable reaction rate  $R_{i(obs)}$ , without external concentration and temperature gradients using the Mears [34] criteria are:

$$\frac{R_{i(obs)} d_p}{k_g C_g} < 0.15 \quad (3)$$

$$\frac{E_a R_{i(obs)} \Delta H_r d_p}{h_f R T^2} < 0.15 \quad (4)$$

Considering a very exothermic reaction such as CO oxidation ( $\Delta H_r = -298$  kJ/mol), for a reaction conditions of CO(1%) + O<sub>2</sub>(2%) balance He, at 298 K and 1 atm, and considering an activation energy  $E_a = 100$  kJ, the maximum observable reaction rates will be  $R_{i(obs)} < 9.1 \times 10^{-3}$  mol/(cm<sup>3</sup> s) for avoiding external mass transfer limitations and  $R_{i(obs)} < 6.3 \times 10^{-5}$  mol/(cm<sup>3</sup> s) for avoiding external



heat transfer limitations. Then, for 100% conversion, the observed reaction rate is  $6.8 \times 10^{-6}$  mol/(cm<sup>3</sup> s) which satisfies the imposed criteria. Nonetheless, the calculations must be repeated for each specific experiment and determine the absence of mass transfer limitations.

**3.2.3.2. Intra-particle mass and heat transfer.** The analysis of the internal transfer phenomena is made based on the Weisz-Prater criteria [34]:

$$\eta\phi^2 = \frac{R_{i(obs)}d_p^2}{D_{ef}C_g} < 0.1 \quad (5)$$

$$\gamma\beta_i(\eta\phi^2) = \left(\frac{E_a}{RT}\right)\left(\frac{\Delta H_r D_{ef} C_g}{\lambda_{ef} T}\right)\left(\frac{R_{i(obs)}d_p^2}{D_{ef} C_g}\right) < 0.1 \quad (6)$$

where,  $D_{ef}$  (estimated in  $2.5 \times 10^{-6}$  m<sup>2</sup>/s) is the effective diffusion coefficient, and  $\lambda_{ef}$  (estimated in 0.4 W/(m K)) is the effective thermal conductivity. Then, the maximum observed reaction rates will be  $R_{i(obs)} < 1 \times 10^{-5}$  mol/(cm<sup>3</sup> s) for the internal mass transfer limitation criterion and  $R_{i(obs)} < 1.5 \times 10^{-4}$  mol/(cm<sup>3</sup> s) for the heat transfer limitation criterion, being both higher than the reaction rate calculated.

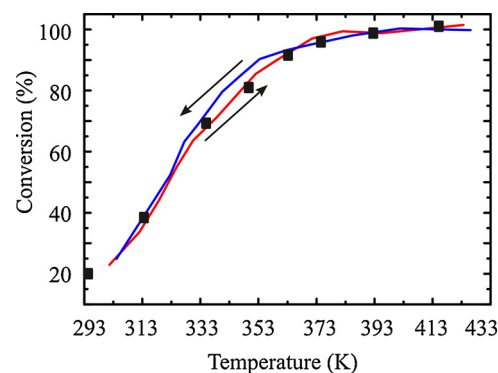
**3.2.3.3. Internal and external mass transfer under non-steady state.** As stated in the introduction section, transient experiment provides essential spectroscopic information for the understanding of reaction mechanisms. For instance, periodic switching of reactants composition in a concentration modulation (c-MES) experiment, must be performed in absence of mass transport limitation in order to get quantitative spectrokinetic data. In this case, the reaction rate and the adsorption capacity of the catalyst influence in the response. Moulijn et al. [36] developed criteria to examine the mass transfer in transient experiments. Analyzing the case of a porous catalyst where a first-order surface reaction occurs and where there is accumulation on the surface, they determined a criterion using the Carberry number  $Ca = \frac{0.15 R_{i(obs)} d_p}{k_g C_g}$ , the Sherwood number  $Sh = \frac{k_g d_p}{D_{ef}}$  and the dimensionless time  $\tau_{in} = \frac{D_{ef}}{\varepsilon_p R^2}$ . Where,  $\varepsilon_p$  is the particle porosity. The authors studied the time needed to achieve an average concentration in the catalyst of 90% of the concentration in the gas phase. To fulfill the criteria, the dimensionless time must be larger than 0.25 for a  $Sh$  larger than 5. Under the example of CO oxidation used before, the time ( $t$ ) must be larger than  $1.2 \times 10^{-3}$  s, that is a value two orders of magnitude smaller than the residence time of the cell.

Summarizing, the combination of small particles (0.1 mm), the small volume of the catalyst bed in the cell (90  $\mu$ L) and the use of high flow rates produces that the filling time of the cell is much longer than the time necessary for set the stationary concentration profile in the catalyst particle.

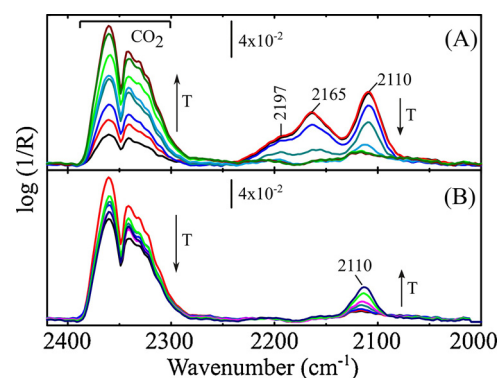
### 3.3. Case of study: CO oxidation on Au/CeO<sub>2</sub>

The developed DRIFT microreactor/cell designed and characterized was used for study the CO oxidation on a gold supported on cerium oxide catalyst. Fig. 6 shows the light-off curve for the CO oxidation during the heating and cooling on a Au/CeO<sub>2</sub> catalyst studied simultaneously by DRIFT and MS using the new DRIFT microreactor. Full points in the figure represent the conversion measured using a conventional 1/4" diameter tubular microreactor [33]. It is observed that for a temperature of 303 K the conversion is 22%, increasing progressively until reaching 100% conversion at 378 K. The temperature for 50% conversion ( $T_{50}$ ) was 322 K with a  $R_{CO} = 3.8$   $\mu$ mol/s/g<sub>cat</sub>. The results show an excellent agreement between both independent measurements, confirming that the cell behaves as a conventional plug-flow microreactor.

Fig. 7A and B show the IR spectra in the 2400 to 2000 cm<sup>-1</sup> region obtained during the heating and cooling of the DRIFT cell. It is clearly observed the increase of the CO<sub>2</sub> signal in the gas phase when the



**Fig. 6.** Light-off curve for the CO oxidation, flowing CO(1%)+O<sub>2</sub>(0.6%)/He (50 mL/min, 48.9 mg Au/CeO<sub>2</sub>). The red curve is during the temperature increase (5 °C/min) and the blue one is for the cooling ramp. The points in the figure represent the conversions measured using a conventional through-flow microreactor (For interpretation of the references to colour in this figure legend, the reader is referred to the web version of this article.).

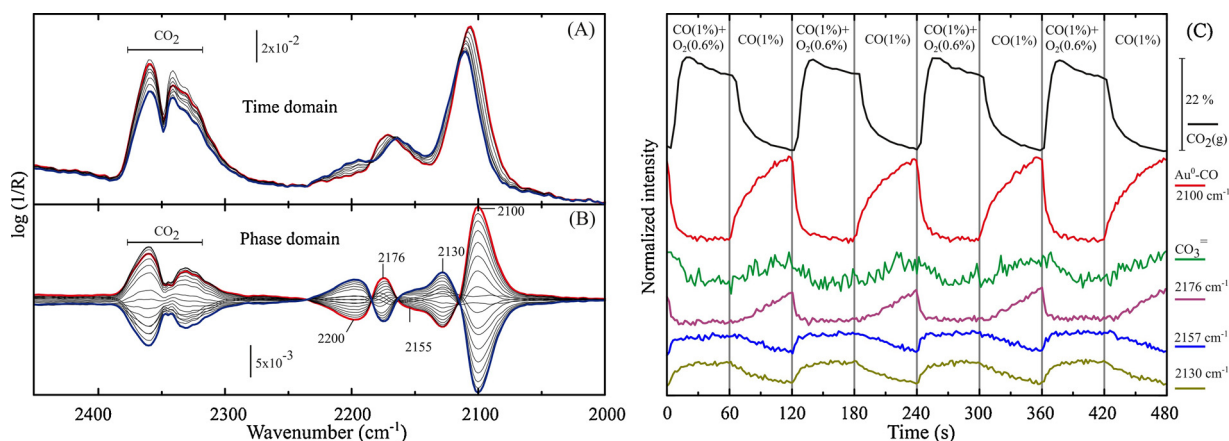


**Fig. 7.** DRIFT spectra collected during the CO oxidation, flowing CO(1%)+O<sub>2</sub>(0.6%)/He (50 mL/min). The spectra were collected during (A) the heating from 303 to 423 K (5 °C/min) and (B) the cooling from 423 to 303 K.

temperature increases, as well as the evolution of the signals in the carbonyl zone. During the heating, the decrease in the band intensities at 2165 cm<sup>-1</sup> assigned to CO adsorbed on Au<sup>+</sup>δ sites [37–45] and at 2110 cm<sup>-1</sup> assigned to CO adsorbed on Au<sup>0</sup> [37–45] was recorded. In addition, a signal was registered at 2197 cm<sup>-1</sup> which could be assigned to residual isocyanate groups of the precursor used in the preparation of the catalyst [33]. During the cooling step, the signal at 2110 cm<sup>-1</sup> corresponding to CO on metallic Au is recovered, and a shoulder appears at ca. 2125 cm<sup>-1</sup>, which is assigned to O-Au<sup>+</sup>-CO surface species [37–45]. During the experiments, CO(g) was not detected in the DRIFTS spectra, since the path length in the gas-phase is negligible (Fig. S5). It is also noted that the recorded infrared signals have an excellent signal-to-noise ratio.

In order to analyze in more detail the role of the assigned surface species, c-MES experiments were performed exchanging between CO (1%)/He and CO(1%)+O<sub>2</sub>(0.6%)/He; in other words, modulating the O<sub>2</sub> concentration and keeping the CO partial pressure constant. Fig. 8A and B show the time-resolved and the phase-resolved spectra (after PSD analysis), respectively, during a complete cycle ( $\omega = 16.67$  mHz). It can be seen that the changes in the time-resolved IR signals are relatively small. After applying the PSD algorithm, the signals that are affected by the stimulus are clearly distinguished: at 2200, 2176, 2155, 2130 and 2100 cm<sup>-1</sup> (Fig. 8B).

The signals at 2176 and 2100 cm<sup>-1</sup> are in-phase with the presence of only CO in the cell (that is without oxygen). Conversely, CO<sub>2</sub>(g) production and the increase of the signals at 2200, 2155 and 2130 cm<sup>-1</sup> are in phase with the reaction mixture. The band at ca.



**Fig. 8.** Time domain spectra (A) and phase domain spectra (B) during the change from CO(1%) to CO(1%) + O<sub>2</sub>(0.6%) ( $\omega = 16.67$  mHz;  $Q = 50$  mL/min;  $T = 303$  K). (C) Evolution of the CO<sub>2</sub> concentration at the cell exit ( $m/e = 44$ ) and the intensity of the integrated IR selected bands during the experiment.

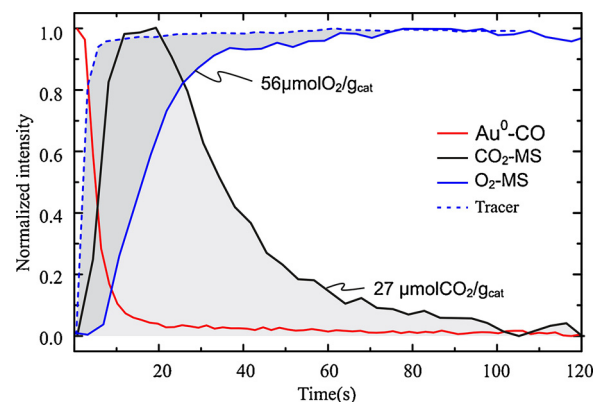
2130  $\text{cm}^{-1}$  can also have some contribution from the forbidden electronic transition  ${}^2F_{5/2} \rightarrow {}^2F_{7/2}$  of  $\text{Ce}^{3+}$  (reduced surface sites) [46,47] as was pointed out in similar catalytic systems [48,49]. However it is important to note that the band at 2130  $\text{cm}^{-1}$  decreases (see Fig. 8B and C) when CO(1%)/He is fed in the cell, that is under reducing condition (e.g. it is out-of-phase with the CO feed), and the signal increases when the reaction mixture is fed. Then, the band is mainly assigned to O-Au<sup>δ+</sup>-CO species [43–45], even when some minor amount of  $\text{Ce}^{+3}$  could also be contributing.

Fig. 8C shows the simultaneous evolutions of the produced CO<sub>2</sub> (signal  $m/e = 44$ ) and the integrated intensities of the IR bands of surface species previously assigned. After the change from CO/He to the reaction mixture CO + O<sub>2</sub>/He, the CO<sub>2</sub> production increases going through a maximum due to the rapid oxidation of adsorbed Au-CO species. The higher initial CO<sub>2</sub> production is partially due to a higher of CO coverage under CO/He, but also a similar behavior was previously reported [37] and attributed to an inhibition by products, due to the adsorption of CO<sub>2</sub> on oxygen sites at the metal-support interface. During the reaction, the signals assigned to O-Au<sup>δ+</sup>-CO species increase, and later decrease when the O<sub>2</sub> is eliminated from the feed, while the Au<sup>0</sup>-CO signal rises.

A complementary set of c-MES experiments were performed changing from O<sub>2</sub>(0.6%)/He to CO(1%)/O<sub>2</sub>(0.6%)/He and CO(1%)/He to O<sub>2</sub>(0.6%)/He (results not shown). Signals at 2100 and 2176  $\text{cm}^{-1}$  were not observed and only the signals at 2165 and 2110  $\text{cm}^{-1}$  were distinguished. This is consistent with the assignments made, since only the signals attributed to CO interaction with O<sub>2</sub> were modified. These experiments show the capability of the cell/microreactor to perform fast transient experiments in order to assign signals and to correlate kinetic and spectroscopic data.

Finally, the transient -in a step experiment- oxidation of pre-adsorbed CO oxidation on the catalyst was studied in order to demonstrate the potentiality for quantify surface concentrations with this experimental set-up. Fig. 9 shows the normalized DRIFT and MS signals during the change from CO(1%)/He to O<sub>2</sub>(0.6%)/He. It is observed that the Au<sup>0</sup>-CO signal at 2110  $\text{cm}^{-1}$  (red curve) rapidly decays and disappears in ca. 20 s (note that the residence time of the cell is 0.11 s for this case). At the same time, the production of CO<sub>2</sub>(g) (black curve) is recorded, which reaches a maximum at approximately 18 s, and then slowly decays showing the complete consumption of adsorbed CO on the catalyst. The signal of O<sub>2</sub>(g) ( $m/e = 32$ , blue curve) gradually grows until reaching the maximum in ca. 80 s, but presenting a delay as compared with the signal a blank experiment without reaction).

The integrated temporal evolution of the calibrated MS signals allows quantifying the amount of reactants consumed and produced during the reaction, taking into account that the designed DRIFT cell



**Fig. 9.** Time evolution of the infrared signal of Au-CO (2110  $\text{cm}^{-1}$ ) and MS signals of CO ( $m/e = 28$ ), O<sub>2</sub> ( $m/e = 32$ ) and CO<sub>2</sub> ( $m/e = 44$ ) after exchanging from CO(1%)/He to O<sub>2</sub>(0.6%)/He ( $Q = 50$  mL/min;  $T = 303$  K) on the Au/CeO<sub>2</sub> catalyst.

behaves as a true plug-flow micro-reactor. Then, during the CO to O<sub>2</sub> exchange experiment, 27 μmol/g<sub>cat</sub> of CO<sub>2</sub>(g) was produced, and 56 μmol/g<sub>cat</sub> of O<sub>2</sub> were consumed. In a supplementary experiment the amount of CO adsorbed on gold sites (see Figure S6 in Supplementary Information) was 25 μmol/g<sub>cat</sub>. Then, the amount of CO<sub>2</sub> produced is in perfect agreement with the amount of CO adsorbed on gold sites. Note that the signal of Au-CO at 2110  $\text{cm}^{-1}$  was the main band formed during the CO adsorption and consumed when the cell was fed with oxygen.

The total amount of O<sub>2</sub> consumed corresponds to the CO<sub>2</sub> produced (CO<sub>2 rxn</sub>) and the O<sub>2</sub> adsorbed on the catalyst (O<sub>2 ads</sub>). Then, the amount of O<sub>2</sub> that remains adsorbed on the catalyst was estimated by a balance.

$$O_2(\text{consumed}) = O_{2\text{ads}} + \frac{1}{2}CO_{2\text{rxn}} \quad (7)$$

$$56 \mu\text{mol} = O_{2\text{ads}} + \frac{1}{2}27 \mu\text{mol} \quad (8)$$

Thus, it can be estimated that approximately 42.5 μmol/g<sub>cat</sub> of O<sub>2</sub>, or 85 μmol/g<sub>cat</sub> of Os, remain adsorbed on the catalyst. This amount can be normalized by the catalyst area giving 1.5 μmol O<sub>2</sub>/m<sup>2</sup><sub>cat</sub>, which is in reasonable agreement with the quantity reported by Behm and co-workers [50,51] of 1.66 μmol O<sub>2</sub>/m<sup>2</sup><sub>cat</sub> on Au/CeO<sub>2</sub> using O<sub>2</sub> multi-pulse experiments in a temporal analysis of products (TAP) reactor.

Altogether, the presented experiments and results show the potential of the designed cell to perform quantitative experiments.

#### 4. Conclusions

A DRIFT cell/microreactor was constructed and characterized. The cell design features a plug flow reactor, eliminates dead volume and temperature gradients, problems usually present in the most commonly used DRIFT cells. The mass and heat transport phenomena were characterized and chemical engineering criteria were fulfilled in order to perform kinetic data acquisition under chemical control conditions. The cell allows the fast tracking of infrared signals from surface species and their correlation with the mass spectrometer gas quantification during steady state Operando experiments and transient experiments in a quantitative manner.

As a proof of concept, the CO oxidation reaction on a well characterized Au/CeO<sub>2</sub> catalyst was performed in order to validate the performance of the new DRIFT cell. Light-off curves were identical to those obtained using a conventional plug-flow reactor and the recorded infrared signals possess an excellent signal-to noise ratio. C-MES experiments, combined with PSD spectral analysis, allowed to follow the evolution of surface species during reaction and their correlation with the concentration of reactants and products in the gas phase in a quantitative manner. Moreover, step experiments allows the quantification of surface species combining DRIFT and MS information.

It is expected that the DRIFT cell presented here will allow the development of quantitative spectrokinetic analysis of surface reactions under true operando methodology.

#### Acknowledgements

Financial support from the Consejo Nacional de Investigaciones Científicas y Técnicas (CONICET)PIP-2014-11220130100086CO and Agencia Nacional para la Promoción de la Ciencia y Tecnología of Argentina (ANPCyT)PICT-2014-0497 is gratefully acknowledged. A.A. thanks CONICET for the fellowship received to carry out this work.

#### Appendix A. Supplementary data

Supplementary material related to this article can be found, in the online version, at doi:<https://doi.org/10.1016/j.mcat.2018.07.003>.

#### References

- M.V. Martínez-Huerta, G.G. Deo, J.L. Fierro, M.A. Bañares, Operando Raman-GC study on the structure–activity relationships in V<sup>5+</sup>/CeO<sub>2</sub> catalyst for ethane oxidative dehydrogenation: the formation of CeVO<sub>4</sub>, *J. Phys. Chem. C* 112 (2008) 11441–11447.
- S.J. Tinnemans, J.G. Mesu, K. Kervinen, T. Visser, T.A. Nijhuis, A.M. Beale, D.E. Keller, A.M.J. van der Eerden, B.M. Weckhuysen, Combining operando techniques in one spectroscopic-reaction cell: New opportunities for elucidating the active site and related reaction mechanism in catalysis, *Catal. Today* 113 (2006) 3–15.
- M.A. Newton, Applying dynamic and synchronous DRIFTS/EXAFS to the structural reactive behaviour of dilute ( $\leq 1$  wt%) supported Rh/Al<sub>2</sub>O<sub>3</sub> catalysts using quick and energy dispersive EXAFS, *Top. Catal.* 52 (2009) 1410–1424.
- C.M.A. Parlett, C.V. Gaskell, J.N. Naughton, M.A. Newton, K. Wilson, A.F. Lee, Operando synchronous DRIFTS/MS/XAS as a powerful tool for guiding the design of Pd catalysts for the selective oxidation of alcohols, *Catal. Today* 205 (2013) 76–85.
- G.L. Chiarello, M. Nachteggall, V. Marchionni, L. Quaroni, D. Ferri, Adding diffuse reflectance infrared fourier transform spectroscopy capability to extended x-ray-absorption fine structure in a new cell to study solid catalysts in combination with a modulation approach, *Rev. Sci. Instrum.* 85 (2014) 074102.
- T.A. Nijhuis, S.J. Tinnemans, T. Visser, B.M. Weckhuysen, Operando spectroscopic investigation of supported metal oxide catalysts by combined time-resolved UV-VIS/Raman/on-line mass spectrometry, *Phys. Chem. Chem. Phys.* 5 (2003) 4361–4365.
- A. Brückner, E. Kondratenko, Simultaneous operando EPR/UV-vis/laser-Raman spectroscopy — A powerful tool for monitoring transition metal oxide catalysts during reaction, *Catal. Today* 113 (2006) 16–24.
- J. Ryzkowski, IR spectroscopy in catalysis, *Catal. Today* 68 (2001) 263–381.
- R.P. Eischens, S.A. Francis, W.A. Pliskin, The effect of surface coverage on the spectra of chemisorbed CO, *J. Phys. Chem.* 60 (1956) 194–201.
- S.E. Collins, M.A. Baltanás, A.L. Bonivardi, An infrared study of the intermediates of methanol synthesis from carbon dioxide over Pd/ $\beta$ -Ga<sub>2</sub>O<sub>3</sub>, *J. Catal.* 226 (2004) 410–421.
- L.J. Burcham, M. Badlani, I.E. Wachs, The origin of the ligand effect in metal oxide catalysts: novel fixed-bed in situ infrared and kinetic studies during methanol oxidation, *J. Catal.* 203 (2001) 104–121.
- Y. Yang, R.S. Disselkamp, J. Szanyi, C.H.F. Peden, C.T. Campbell, J.G. Goodwin, Design and operating characteristics of a transient kinetic analysis catalysis reactor system employing in situ transmission fourier transform infrared, *Rev. Sci.: Instrum.* 77 (2006) 094104.
- T. Lesage, C. Verrier, P. Bazin, J. Saussey, M. Daturi, Studying the NO<sub>x</sub>-trap mechanism over a Pt-Rh/Ba/Al<sub>2</sub>O<sub>3</sub> catalyst by operando FTIR spectroscopy, *Phys. Chem. Chem. Phys.* 5 (2003) 4435–4440.
- S.B. Rasmussen, M.A. Bañares, P. Bazin, J. Due-Hansen, P. Avila, M. Daturi, Monitoring catalysts at work in their final form: spectroscopic investigations on a monolithic catalyst, *Phys. Chem. Chem. Phys.* 14 (2012) 2171–2177.
- S.B. Rasmussen, S. Perez-Ferreras, M.A. Bañares, P. Bazin, M. Daturi, Does pelletizing catalysts influence the efficiency number of activity measurements? Spectrochemical engineering considerations for an accurate operando study, *ACS Catal.* 3 (2013) 86–94.
- R.F. Hicks, C.S. Kellner, B.J. Savatsky, W.C. Hecker, A.T. Bell, Design and construction of a reactor for in situ infrared studies of catalytic reactions, *J. Catal.* 71 (1981) 216–218.
- F.C. Meunier, A. Goguet, S. Shekhtman, D. Rooney, H. Daly, A modified commercial DRIFTS cell for kinetically relevant operando studies of heterogeneous catalytic reactions, *Appl. Catal. A* 340 (2008) 196.
- V. Dal Santo, C. Dossi, A. Fusi, R. Psaro, C. Mondelli, S. Recchia, Fast transient infrared studies in material science: development of a novel low dead-volume, high temperature DRIFTS cell, *Talanta* 66 (2005) 674–682.
- M.M. Schubert, T.P. Häring, G. Bräth, H.A. Gasteiger, R.J. Behm, New DRIFTS cell design for the simultaneous acquisition of IR spectra and kinetic data using on-line product analysis, *Appl. Spectrosc.* 55 (2001) 1537–1543.
- B. Li, R.D. Gonzalez, Design and construction of a DRIFTS accessory and an in situ heatable sample cell, *Appl. Spectrosc.* 52 (1998) 1488–1491.
- C. Daniel, M.O. Clarté, S.P. Teh, O. Thion, H. Provendier, A.C. Van Veen, B.J. Beccard, Y. Schuurman, C. Mirodatos, Spatially resolved catalysis in micro-structured reactors by IR spectroscopy: CO oxidation over mono- and bifunctional Pt catalysts, *J. Catal.* 272 (2010) 55–64.
- A. Urakawa, N. Maeda, A. Baiker, Space- and time-resolved combined DRIFT and raman spectroscopy: monitoring dynamic surface and bulk processes during NO<sub>x</sub> storage reduction, *Angew. Chem. Int. Ed.* 47 (2008) 9256–9259.
- F.C. Meunier, The design and testing of kinetically-appropriate operando spectroscopic cells for investigating heterogeneous catalytic reactions, *Chem. Soc. Rev.* 39 (2010) 4602–4614.
- A. Aguirre, S.E. Collins, Selective detection of reaction intermediates using concentration-modulation excitation DRIFT spectroscopy, *Catal. Today* 205 (2013) 34–40.
- D. Baurecht, U.P. Fringeli, Quantitative modulated excitation fourier transform infrared spectroscopy, *Rev. Sci. Instrum.* 72 (2001) 3782.
- E.E. Orтели, J. Wambach, A. Wokaun, *Appl. Catal. A-Gen.* 192 (2000) 137–152.
- E.E. Orтели, J. Wambach, A. Wokaun, *Appl. Catal. A-Gen.* 216 (2001) 227–241.
- A. Urakawa, T. Bürgi, A. Baiker, Kinetic analysis using square-wave stimulation in modulation excitation spectroscopy: mixing property of a flow-through PM-IRRAS cell, *Chem. Phys.* 324 (2006) 653–658.
- A. Urakawa, T. Bürgi, A. Baiker, *Chem. Eng. Sci.* 63 (2008) 4902–4909.
- P. Müller, I. Hermans, Applications of modulation excitation spectroscopy in heterogeneous catalysis, *Ind. Eng. Chem. Res.* 56 (2017) 1123–1136.
- F. Meunier, D. Reid, A. Goguet, S. Shekhtman, C. Hardacre, R. Burch, W. Deng, M. Flytzani-Stephanopoulos, Quantitative analysis of the reactivity of formate species seen by DRIFTS over a Au/Ce(La)O<sub>2</sub> water-gas shift catalyst: first unambiguous evidence of the minority role of formates as reaction intermediates, *J. Catal.* 247 (2007) 277–287.
- H. Li, M. Rivallan, F. Thibault-Starzyk, A. Travert, F.C. Meunier, Eff;ective bulk and surface temperatures of the catalyst bed of FT-IR cells used for in situ and operando studies, *Phys. Chem. Chem. Phys.* 15 (2013) 7321–7327.
- J. Vecchiotti, S.E. Collins, J.J. Delgado, M. Małecka, E. del Rio, X. Chen, S. Bernal, A.L. Bonivardi, Gold catalysts supported on Cerium–Gallium mixed oxide for the carbon monoxide oxidation and water gas shift reaction, *Top. Catal.* 54 (2011) 201–209.
- G.F. Froment, K.B. Bischoff, J. De Wilde, *Chemical Reactor Analysis and Design*, 3rd ed, Wiley & Sons, New York, 2011.
- R.B. Bird, W.E. Stewart, E.N. Lightfoot, *Transport Phenomena*, 2da ed, Wiley & Sons, New York, 2002.
- F.H.M. Dekker, A. Bliet, F. Kapteijn, J.A. Moulijn, Analysis of mass and heat transfer in transient experiments over heterogeneous catalysts, *Chem. Eng. Sci.* 50 (1995) 3573–3580.
- E. del Río, S.E. Collins, A. Aguirre, X. Chen, J.J. Delgado, J.J. Calvino, S. Bernal, Reversible deactivation of a Au/Ce<sub>0.62</sub>Zr<sub>0.38</sub>O<sub>2</sub> catalyst in CO oxidation: a systematic study of CO<sub>2</sub>-triggered carbonate inhibition, *J. Catal.* 316 (2014) 210–218.
- A. Fielicke, G. von Helden, G. Meijer, D.B. Pedersen, B. Simard, D.M. Rayner, Gold cluster carbonyls: saturated adsorption of CO on gold cluster cations, vibrational spectroscopy, and implications for their structures, *J. Am. Chem. Soc.* 127 (2005) 8416–8423.
- A. Aguirre, C.E. Barrios, A. Aguilar-Tapia, R. Zanella, M.A. Baltanás, S.E. Collins, In-situ DRIFT study of Au–Ir/Ceria catalysts: activity and stability for CO oxidation, *Top. Catal.* 59 (2016) 347–356.
- T. Tabakova, F. Boccuzzi, M. Manzoli, D. Andreeva, FTIR study of low-temperature water-gas shift reaction on gold/ceria catalyst, *Appl. Catal. A: Gen.* 252 (2003)

- 385–397.
- [41] T. Tabakova, F. Boccuzzi, M. Manzoli, J.W. Sobczak, V. Idakiev, D. Andreeva, Effect of synthesis procedure on the low-temperature WGS activity of Au/ceria catalysts, *Appl. Catal. B: Environ.* 49 (2004) 73–81.
- [42] M. Manzoli, F. Boccuzzi, A. Chiorino, F. Vindigni, W. Deng, M. Flytzani-Stephanopoulos, Spectroscopic features and reactivity of CO adsorbed on different Au/CeO<sub>2</sub> catalysts, *J. Catal.* 245 (2007) 308–315.
- [43] G. Avgouropoulos, M. Manzoli, F. Boccuzzi, T. Tabajova, J. Papavasiliou, T. Ioannides, V. Idakiev, Catalytic performance and characterization of Au/doped-ceria catalysts for the preferential CO oxidation reaction, *J. Catal.* 256 (2008) 237–315.
- [44] I. Green, W. Tang, M. Neurock, J.T. Yates, Spectroscopic observation of dual catalytic sites during oxidation of CO on a Au/TiO<sub>2</sub> catalyst, *Science* 333 (2011) 736–739.
- [45] I. Green, W. Tang, M. McEntee, M. Neurock, J.T. Yates, Inhibition at perimeter sites of Au/TiO<sub>2</sub> oxidation catalyst by reactant oxygen, *J. Am. Chem. Soc.* 134 (2012) 12717–12723.
- [46] C. Binet, A. Badri, L.C. Lavalley, A spectroscopic characterization of the reduction of ceria from electronic transitions of intrinsic point defects, *J. Phys. Chem.* 98 (1994) 6392–6398.
- [47] C. Binet, M. Daturi, M.J.C. Lavalley, IR study of polycrystalline ceria properties in oxidised and reduced states, *Catal. Today* 50 (1999) 207–225.
- [48] H. Dalya, J. Nia, D. Thompsett, F.C. Meunier, On the usefulness of carbon isotopic exchange for the operando analysis of metal–carbonyl bands by IR over ceria-containing catalysts, *J. Catal.* 254 (2008) 238–243.
- [49] S.E. Collins, J.M. Cies, E. Del Río, J.M. Pintado, S. Trasobares, J.J. Calvino, S. Bernal, Hydrogen interaction with a ceria-zirconia supported gold catalyst. Influence of CO co-adsorption and pre-treatment conditions, *J. Phys. Chem. C* 111 (2007) 14371–14379.
- [50] L. Wang, D. Widmann, R.J. Behm, Reactive removal of surface oxygen by H<sub>2</sub>, CO and CO/H<sub>2</sub> on a Au/CeO<sub>2</sub> catalyst and its relevance to the preferential CO oxidation (PROX) and reverse water gas shift (RWGS) reaction, *Catal. Sci. Technol.* 5 (2015) 925–941.
- [51] D. Widmann, R.J. Behm, Activation of molecular oxygen and the nature of the active oxygen species for CO oxidation on oxide supported Au catalysts, *Acc. Chem. Res.* 47 (2014) 740–749.